

Influence of erosion and sedimentation on strike-slip fault systems: insights from analogue models

Erwan Le Guerroué^{a,b}, Peter Robert Cobbold^{a,*}

^a Géosciences-Rennes (UMR 6118 du CNRS), Université de Rennes 1, Campus de Beaulieu, 35042 Rennes Cedex, France

^b Geological Institute, ETH-Zentrum, Sonneggstrasse 5, 8092 Zürich, Switzerland

Received 3 February 2005; received in revised form 2 November 2005; accepted 19 November 2005

Abstract

We describe 18 experiments on the formation of strike-slip fault systems in sand. All models were in a rectangular box. A piston imparted strike-slip motion along a basal cut. In some experiments, uplifted areas underwent erosion. In others, all areas were subject to sedimentation.

In experiments without erosion or sedimentation, first to develop were R-faults, at 16° to the basal cut. At later stages, P-faults and Y-faults took over. In section, faults splayed upward, forming flower structures. The splays had reverse components of slip. This was due to dilation, which reached 7% within fault splays. In experiments with erosion but no sedimentation, faults were less steep and accumulated greater amounts of reverse slip. In experiments with erosion and sedimentation, some faults propagated through their syn-kinematic cover, others became buried and inactive, whilst yet others were exposed by erosion. Therefore the average fault dip increased significantly. In experiments with sedimentation but no erosion, early faults propagated, whereas others became buried.

Flower structures in nature have similar features. In areas of sedimentation, fault splays with gentle dips die out at depth, whereas steeper faults penetrate higher. In areas of erosion, strike-slip systems exhibit large amounts of reverse slip on steep bounding faults.

© 2006 Elsevier Ltd. All rights reserved.

Keywords: Strike-slip faults; Erosion; Sedimentation; Analogue models

1. Introduction

Major strike-slip fault systems may accommodate thousands of kilometres of horizontal displacement, juxtaposing very different geological units (Christie-Blick and Biddle, 1985). Commonly, such systems develop within continental crust, close to transcurrent plate boundaries (Sylvester, 1988). Some well-described examples are the San Andreas system of California (Crowell, 1982), the Alpine system of New Zealand (Umhoefer, 2000), the Oca system of Venezuela (Audemard, 1996) and the Levant system of the Middle East (Mart et al., 2005). Other strike-slip systems transfer displacements from one orogenic belt to another. A good example is the Altyn Tagh fault system of central Asia (Cobbold and Davy, 1988).

In the brittle upper crust, strike-slip systems tend to be complex arrays of structures, in which minor faults strike obliquely to the overall trend, are *en échelon* and undergo oblique slip (Tchalenko, 1970; Naylor et al., 1986). In cross-section,

faults tend to be steep at depth and to splay upwards, forming characteristic flower structures (Fig. 1; Harding, 1985; Sylvester, 1988). The conventional wisdom is that standard flower structures form in strike-slip settings and their fault splays have reverse or normal components of slip (Fig. 1a), positive flower structures form in transpressional settings and their fault splays have reverse components of slip (Fig. 1b) and negative flower structures form in transtensional settings and their fault splays have normal components of slip (Fig. 1c).

It is now widely accepted that ongoing erosion and sedimentation influence the shapes of developing growth faults. For example, in an extensional setting, normal growth faults become listric as a result of synchronous deformation and sedimentation (Vendeville and Cobbold, 1988). Similarly, in a compressional setting, reverse faults tend to become steeper towards the surface as a result of ongoing sedimentation in the footwall or erosion of the hanging wall (Davy and Cobbold, 1991; Cobbold et al., 1993; Storti and McClay, 1995; Tondji Biyo, 1995; Barrier et al., 2002; Persson and Sokoutis, 2002). Similar, if less pronounced, responses to sedimentation and erosion occur in transtensional (Rahe et al., 1998; Schreurs and Colletta, 1998) and transpressional settings (Schreurs and Colletta, 1998; Casas et al., 2001). In strike-slip fault systems,

* Corresponding author. Tel.: +33 223236096; fax: +33 223236100.

E-mail address: peter.cobbold@univ-rennes1.fr (P.R. Cobbold).

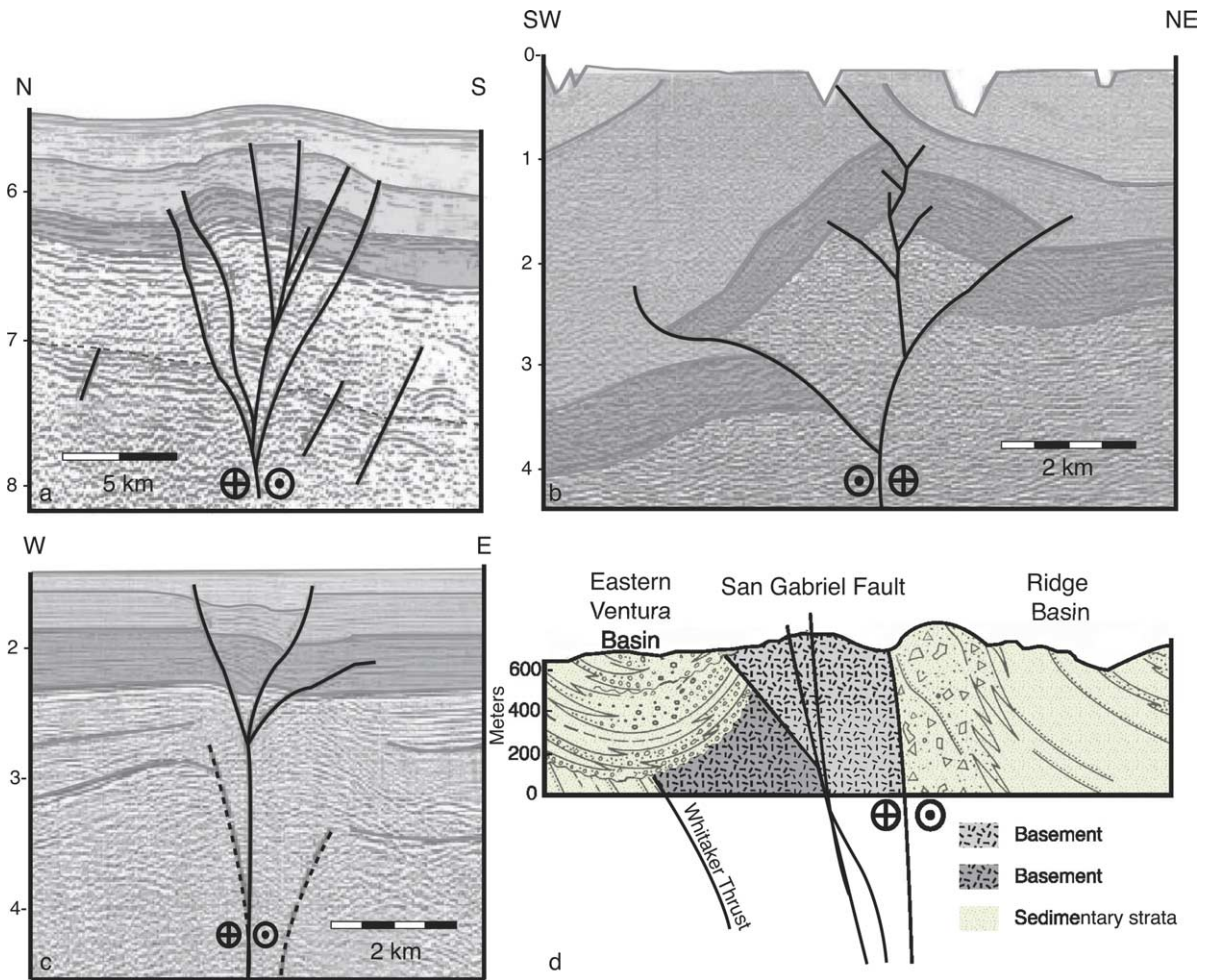


Fig. 1. Flower structures in nature. Seismic profiles (modified after Harding, 1985, 1990) are of positive flower structures from the Aruba Gap Abyssal Plain, Colombia (a) and Ardmore basin (b); and negative flower structure from the Andaman Sea (c). Vertical scale is in seconds of two-way travel time. Geological profile (d) is across San Gabriel fault zone, California (modified after Crowell, 1982). Symbols in circles represent sense of strike-slip (point coming toward observer, cross going away).

where boundary displacements are dominantly horizontal, components of vertical displacement nevertheless occur on internal fault splays. If erosion and sedimentation are coeval with strike-slip deformation (Fig. 1d), one might expect them to have some effects on fault shapes. To explore this possibility is the object of our paper.

Because strike-slip fault systems are complex in three-dimensions and because brittle rocks have non-linear mechanical properties, numerical models of such systems are not yet in an advanced state. In contrast, physical models are well suited to the study of strike-slip fault systems and have greatly progressed in recent years. Mostly they have made use of sand and other granular materials, which yield according to a pressure-dependent Coulomb criterion and form faults as a result of progressive dilation, in ways similar to brittle rocks. Some early experiments concentrated on deformation that was purely strike-slip (Cloos, 1928; Riedel, 1929; Emmons, 1969; Tchalenko, 1970; Naylor et al., 1986), whereas more recent ones have investigated the effects of transpression (Richard and Cobbold, 1989, 1990; Schreurs and Colletta, 1998; Casas et al., 2001; McClay et al., 2004; Viola et al., 2004) and transtension

(Dooley and McClay, 1997; Rahe et al., 1998; Schreurs and Colletta, 1998).

In this paper we describe structures that formed within a sedimentary cover, above a single strike-slip fault in the basement. In the models, sand represented the cover. In some experiments, uplifted areas underwent erosion. In other experiments, all surface areas were subject to sedimentation.

2. Experimental method

As a model material, we used sifted quartz sand from Fontainebleau. This is wind-blown desert sand; the grains are unusually round and smooth. We sieved a batch of Fontainebleau sand, retaining the fraction between 0.4 and 0.5 mm. Sand packs were prepared by pouring sand from a beaker and levelling the top surface with a scraper. The average density was then about 1400 kg m^{-3} .

Dry sand deforms permanently, once the applied shear stress exceeds a critical yield envelope in Mohr space. The envelope is approximately linear, except near the origin, where it curves. The apparent cohesion (intercept on the shear stress axis) is

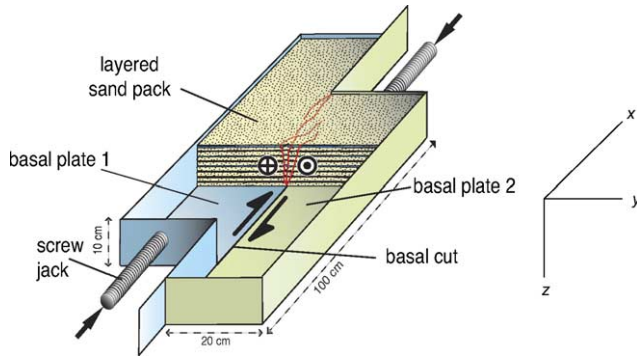


Fig. 2. Experimental apparatus. Box is in two halves. Screw jacks induce sliding along basal cut. This induces flower structure within sand. Notice Cartesian coordinate system (right).

negligible and the angle of internal friction (slope of the Mohr envelope) is more than 45° (Sture et al., 1988; Mourgues and Cobbold, 2003). The yield stress is insensitive to the rate of deformation, provided that inertial forces are negligible. As strain accumulates, the sand dilates and the deformation localizes into discrete shear bands or faults. At the same time, the shear stress decreases by about 15%, from a peak value to a dynamically stable one (Mandl et al., 1977; Sture et al., 1988; Ellis et al., 2004). The dilation may reach 10%, but is more typically 5%. The decrease in density is enough to render the faults visible on X-ray images (Mandl, 1988; Richard et al., 1989; Colletta et al., 1991).

Our models were properly scaled for gravitational forces and stresses (Hubbert, 1937; Horsfield, 1977; Davy and Cobbold, 1988, 1991). The model ratios of length, density and stress were 2×10^{-5} , 0.7 and 1.4×10^{-5} , respectively.

The models were built and deformed in a rectangular box, 1 m long, 40 cm wide and 10 cm deep. Screw jacks, driven by a stepper motor, displaced the two halves of the box horizontally and in opposite senses, causing slip between them (Fig. 2). The amount of slip along the basal cut did not exceed 40 cm. As the sand packs in our experiments were no more than 8 cm thick, the lateral boundaries had little effect on deformation. Instead, the driving forces for deformation in the sand came from the sliding basal plates, which were in frictional contact with the overlying sand. In principle, the vertical gradient of basal shear stress, $\partial\sigma_{xz}/\partial z$, balanced the horizontal gradient of vertical shear stress, $\partial\sigma_{xy}/\partial y$. Thus the shear stress, σ_{xy} , was at a maximum above the basal cut, causing deformation to initiate along that line.

Models were constructed in successive layers of alternating colours, by pouring sand from a beaker and scraping it down to a datum surface. During deformation, photographs of the upper surface were taken at regular time intervals (Fig. 3). At the end of each experiment, the internal structures were photographed on serial sections.

Experiments were in five series, according to the conditions at the upper surface. In Series 1, there was neither erosion nor sedimentation. A square grid of passive coloured markers recorded the progressive deformation (Fig. 4). In Series 2, we

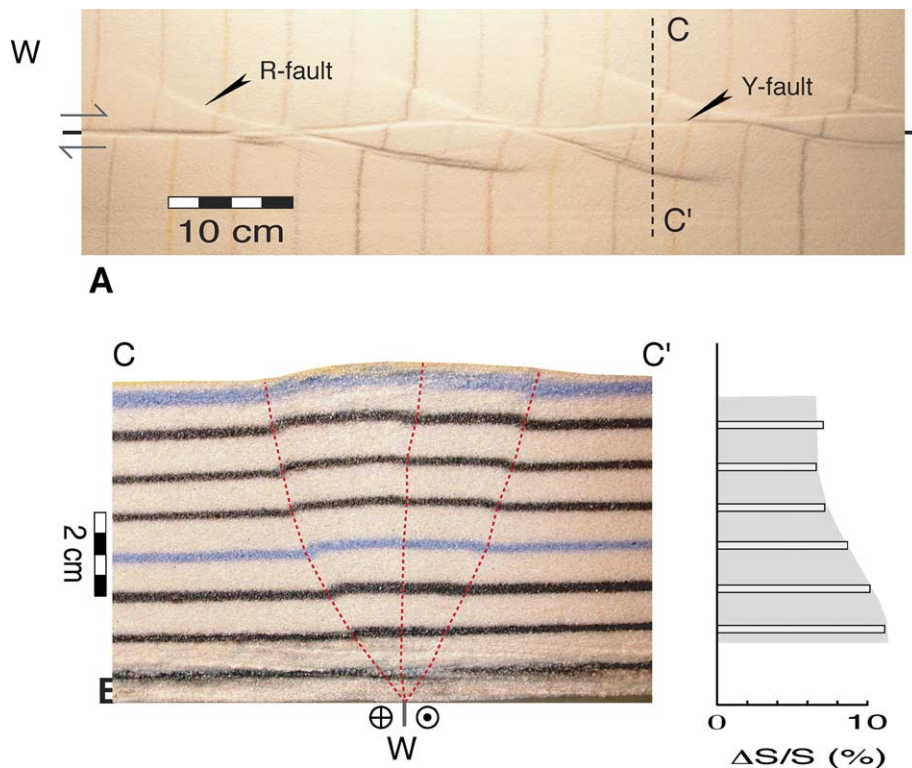


Fig. 3. Typical experimental flower structure (Series 1). Conditions were 5 cm of basal slip and no erosion or sedimentation. At upper surface (a), early R-faults were cut by later Y-faults. In section C–C' (b), faults splayed up through sand from basal cut (W). Notice reverse sense of dip-slip on faults. Bar diagram at right represents dilation (increase in cross-sectional area, ΔS , as percentage of underlying area, S , beneath each layer of flower structure (see text for details).

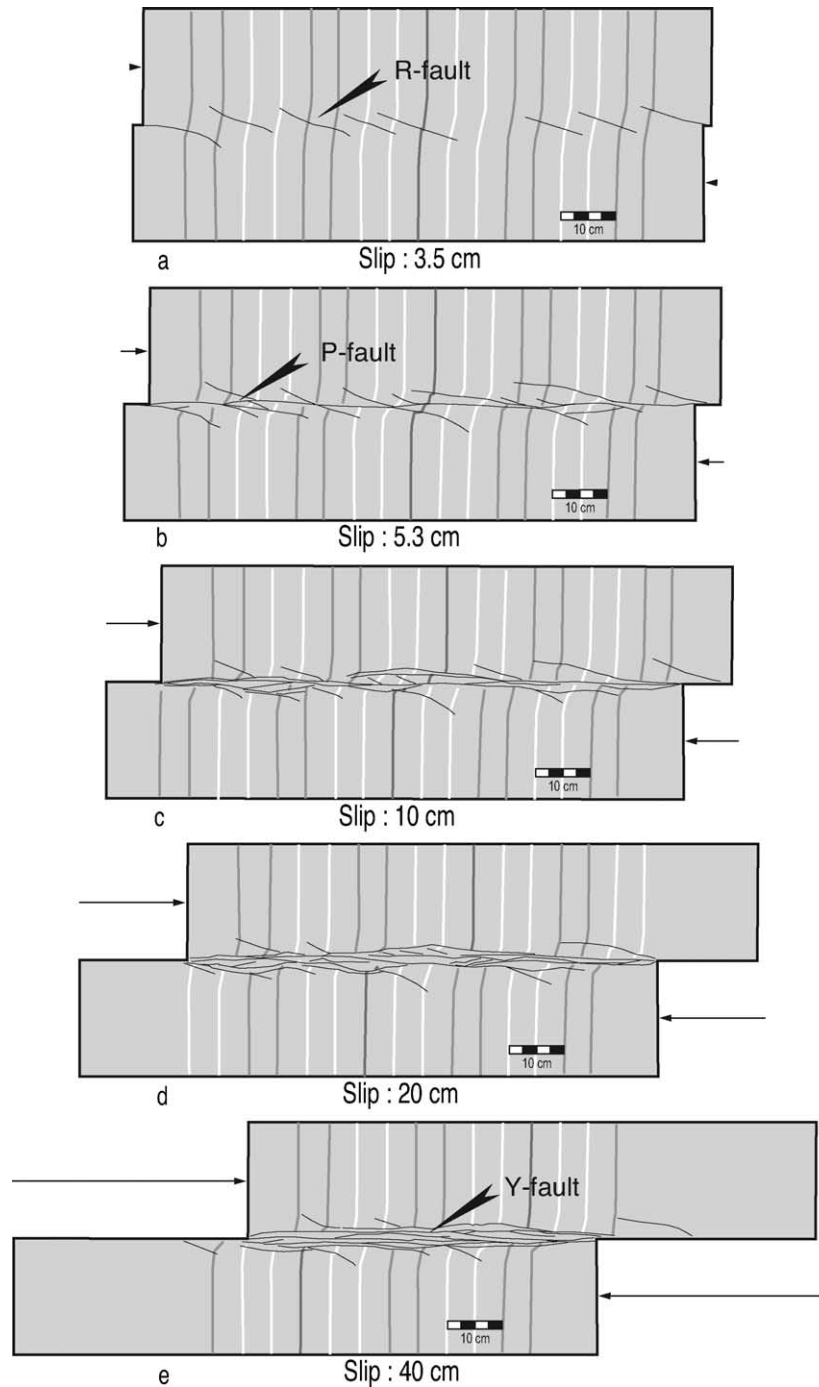


Fig. 4. Deformation at free surface for increasing amounts of basal slip (Series 1). There was no erosion or sedimentation. Passive markers (black, white and grey) acquired right-lateral offsets. Later Y-faults (e) linked or cut earlier R-faults (a) and P-faults (b).

used a vacuum cleaner, fitted with a fine nozzle, to erode all uplifted areas, reducing them to a peneplain. In Series 3, similar episodes of erosion were followed by episodes of uniform sediment supply, during which sand fell in a fine curtain from a travelling hopper. In Series 4, the model was subject to episodic uniform sedimentation, but no erosion. Finally, in Series 5, sedimentation was twice as fast as it was in Series 4. In each of Series 1 to 4, we repeated the experiments for basal slips of 5, 10, 20 and 40 cm (Table 1). This enabled

us to follow the development of structures and to check that the results were broadly reproducible. In Series 5, the basal slips were of 5 and 40 cm only. Despite their limited scope, we include these results for qualitative comparison with the others.

On the photographs of serial sections, we measured for each fault the average dip and the apparent amount of slip from the offset of pre-kinematic layers. We then calculated for each model the average values of fault dip and fault slip and plotted them against the amount of basal slip (Fig. 5).

Table 1
Conditions for the five series of experiments

Total slip (cm)	Series 1 No erosion, no sedimentation	Series 2 Erosion, no sedimentation	Series 3 Erosion, sedimentation	Series 4 Sedimentation, no erosion	Series 5 Rapid sedimentation, no erosion
5	–	Erosion (1 cycle)	Erosion, 2 mm of sedimentation (1 cycle)	2 mm of sedimentation (1 cycle)	10 mm of sedimentation (5 cycles)
10	–	Erosion (3 cycles)	Erosion, 2 mm of sedimentation (3 cycles)	2 mm of sedimentation (3 cycles)	–
20	–	Erosion (3 cycles)	Erosion, 5 mm of sedimentation (3 cycles)	5 mm of sedimentation (3 cycles)	–
40	–	Erosion (5 cycles)	Erosion, 5 mm of sedimentation (5 cycles)	5 mm of sedimentation (5 cycles)	10 mm of sedimentation (5 cycles)

3. Experimental results

3.1. Series 1: no erosion, no sedimentation

This series was done as a standard, for comparison with the others. The results were characteristic of strike-slip faulting in brittle rock and other frictional materials (Cloos, 1928; Riedel, 1929; Skempton, 1966; Tchalenko, 1970; Wilcox et al., 1973; Sylvester, 1988). Similar results have been described before for sand (Emmons, 1969; Naylor et al., 1986; Richard and Cobbold, 1989, 1990; Richard, 1990; Richard et al., 1995; Schöpfer and Steyrer, 2001; Viola et al., 2004).

First to appear were synthetic (right-lateral) Riedel faults (Riedel, 1929), trending at about 16° to the basal cut (R-fault, Figs. 3 and 4). This orientation is predictable from the failure envelope, if the maximal shear stress is parallel to the basal cut, so that all forces balance. At the surface, the areas between en-échelon R-faults rose by as much as 1 cm. A few P-faults formed between the R-faults (Fig. 4). Then a number of Y-faults, parallel to the basement fault, crosscut the earlier R-faults and P-faults.

In cross-section, all faults splayed upwards from the basal cut, forming typical flower structures (Figs. 3 and 6). In three dimensions, the faults were helicoidal (Naylor et al., 1986; Richard, 1990). According to measurements on cross-sections, the average fault dip increased steadily, reaching about 82° for 15 cm of basal slip (Figs. 5 and 6). After that, as the basal slip increased to 20 cm, the dip changed very little. Of all the faults, the most gently dipping were the R-faults. During early stages of deformation, these R-faults had reverse components of dip-slip, but during later stages (after more than 40 cm of basal slip), these reverse components decreased, eventually to zero, and in this sense the R-faults disappeared (Fig. 6), although they did remain as zones of dilation. Simultaneously, Y-faults appeared and they did so with progressively steeper dips. That is why the average dip of all faults increased (Figs. 4–6).

The average amount of reverse slip on all faults (as a percentage of initial model height) increased more steadily, reaching about 8% for 40 cm of basal slip (Figs. 5 and 6). From their strikes, relative to the sense of basal slip, one might have expected the R-faults to have normal components of dip-slip. Nevertheless, all of them had reverse components (as in Richard et al., 1989). Following Schöpfer and Steyrer (2001), we attribute this apparent discrepancy to the positive dilation

that accompanies strain localization and faulting in sand. Along cross-sections, we measured an apparent dilation, which for each layer in the flower structure was the percentage increase, ΔS , in the underlying cross-sectional area, S . This apparent dilation is equal to the true average volumetric dilation beneath each layer, provided that there are (1) no changes in length of the flower structure, (2) no variations in that direction, and (3) no errors due to displacement of material into or out of the plane of section. In one example, the apparent cross-sectional dilation was as much as 7% for an entire flower and 12% for the lower third of the flower, where several major fault strands converged (Fig. 3). However, this section was across the most uplifted part of the flower, that is, the part between two bounding R-faults having large components of reverse slip. In other sections, where faults had negligible reverse components, the dilation was much smaller. By repeating the experiment and using a laser scanner to measure the surface topography at a resolution of 1 mm, we were able to obtain a fully three-dimensional measure of dilation for the entire flower (4%). Thus we estimate the dilation in the major faults to have been more like 7%. It would be pertinent to evaluate this more precisely, by making detailed measurements of density, either on serial sections, or by calibrated X-ray tomography.

3.2. Series 2: erosion, no sedimentation

In Series 2, all uplifted areas underwent episodic erosion, so that little or no relief developed (Table 1; Fig. 6).

During initial stages of deformation, reverse faults had relatively gentle dips (about 60°). During later stages, the early faults disappeared, in the sense that their vertical components of slip became reduced to negligible values. Steep faults replaced them, resulting in narrow flowers. Thus the average dip of faults in cross-section increased rapidly (Fig. 5). However, after 20 cm of basal slip, the average dip stabilized at about 81°. This was the shallowest of all the average dips that we recorded in the experiments.

In contrast, the amount of reverse slip for Series 2 was the highest that we recorded, especially during initial stages of deformation (around 9 and 11% at 10 and 20 cm of slip, respectively; Fig. 6).

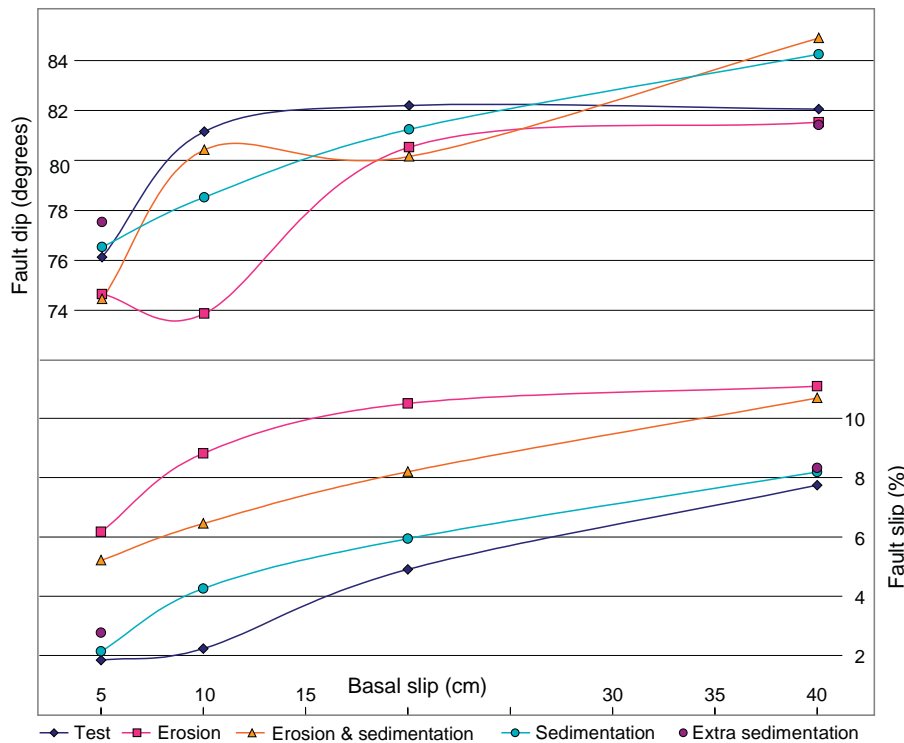


Fig. 5. Fault dip and fault slip versus basal slip, for five series of experiments (key at bottom). Data are from pre-kinematic layers only and have been averaged over entire model. Slip is expressed as percentage of initial model height (8 cm). Estimated errors are 1° (for dips) and 0.5% (for slip).

The narrow flowers and large offsets were probably due to exhumation in areas of erosion.

3.3. Series 3: erosion, sedimentation

In Series 3, episodes of erosion alternated with episodes of uniform sediment supply (Table 1; Fig. 6).

During progressive deformation, some of the early faults propagated through their syn-kinematic cover, others became inactive and buried, whilst yet others were exposed by erosion. The average fault dip increased significantly, especially at early and late stages of deformation and it did not stabilize (Fig. 5).

The average amount of reverse slip was (1) larger than that of Series 1, but (2) smaller than that of Series 2. A likely reason for this was that the amount of exhumation in Series 3 was greater than in Series 1, but less than in Series 2.

3.4. Series 4: sedimentation, no erosion

In Series 4, there was no erosion, but a uniform rate of sediment supply (Table 1; Fig. 6). Relief was moderate, because some of the aggrading grains rolled down slope, exposing hills and filling depressions.

During progressive deformation, some of the early faults propagated through their syn-kinematic cover, whereas others became inactive and buried. The average fault dip increased steadily and did not stabilise (Fig. 5). We tentatively infer that the increasing thickness of overburden during sedimentation

may have suppressed the faults that had gentle dips, whilst favouring the steep faults that had less weight in their hanging walls.

The average amount of reverse slip on faults (expressed as a percentage of initial model height) was a little larger than that of Series 1, but significantly less than that of Series 2 or 3. Again, this may have been due to lack of erosion.

3.5. Series 5: rapid sedimentation, no erosion

In this series of only two experiments (Table 1), rapid sedimentation had little effect on fault slip, but it did generate steep faults in the early stages of deformation (Figs. 5 and 6). Early faults with gentle dips rapidly became buried and inactive, at the expense of steep faults, so that the flower structures became relatively narrow toward their tops (Fig. 7).

4. Discussion

4.1. Comparison of our experiments with previous ones

Our experimental results are comparable in some ways with previous ones. This is particularly true for the standard results of Series 1, which are almost identical to those reported for sand (Emmons, 1969; Tchalenko, 1970; Naylor et al., 1986; Schöpfer and Steyrer, 2001). More generally, the various kinds of faults in our experiments (R, P, and Y) are characteristic of strike-slip systems in nature and in experiment (Tchalenko, 1970; Wilcox et al., 1973; Naylor et al., 1986; Richard, 1990).

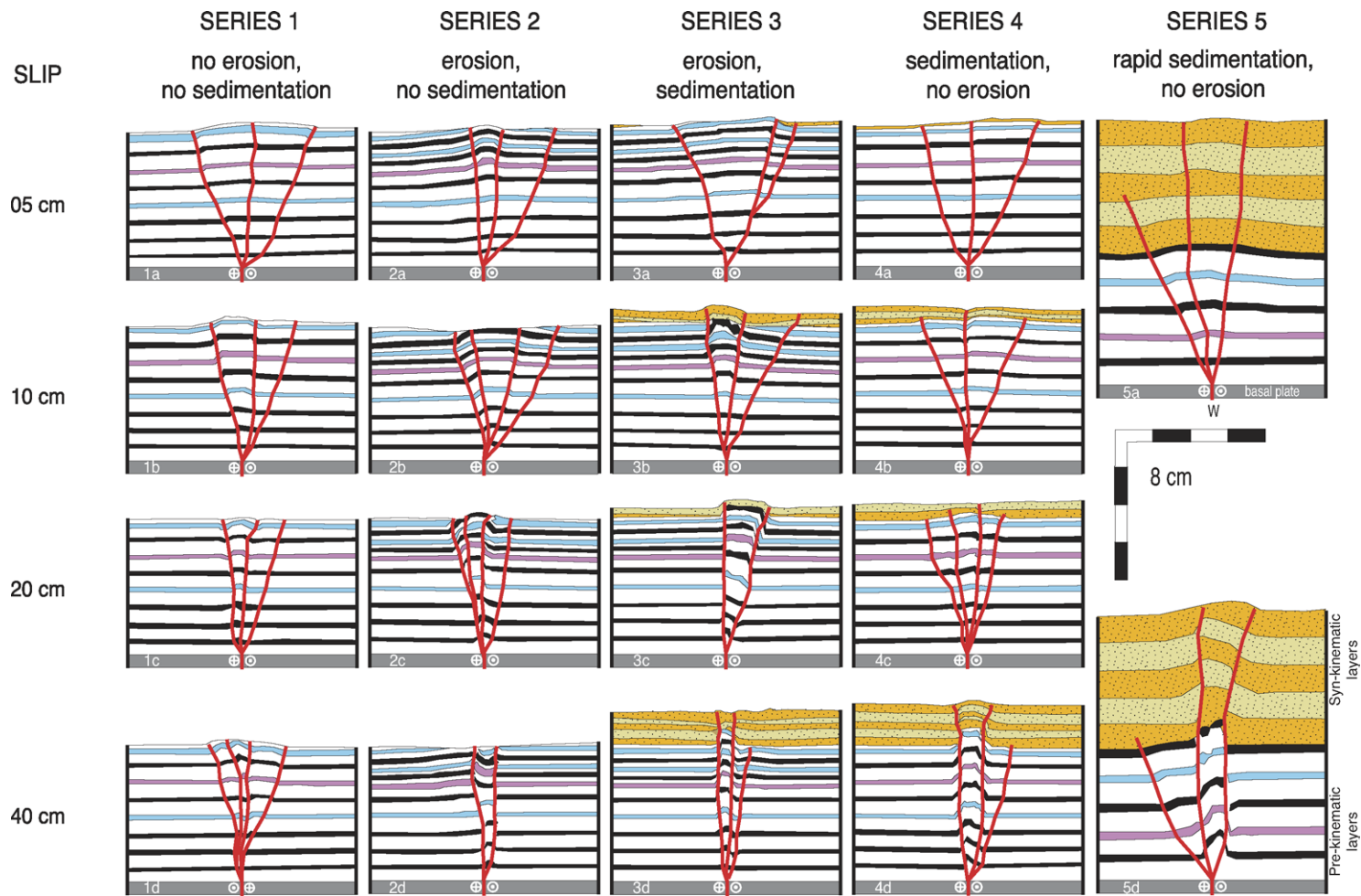


Fig. 6. Array of representative cross-sections. Rows are for amount of slip on basal cut (W): 5 cm (a), 10 cm (b), 20 cm (c) and 40 cm (d). Columns are for experimental conditions: no erosion or sedimentation (1), erosion and no sedimentation (2), erosion and sedimentation (3), sedimentation and no erosion (4), and rapid sedimentation and no erosion (5).

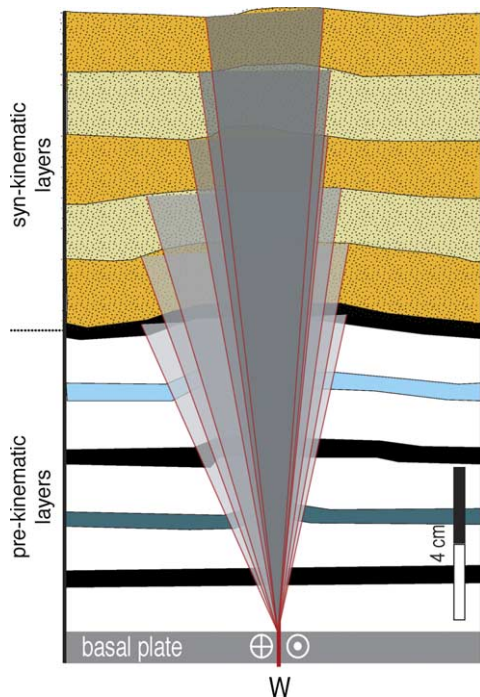


Fig. 7. Diagram illustrating how faults became steeper during sedimentation. Shaded sectors encompass visible faults. Early faults had gentle dips and became inactive. Later faults had steeper dips. Hence flower structure narrows upward.

The new features of our experiments are the effects of erosion and sedimentation on strike-slip systems. Significant effects of erosion and sedimentation had been documented before, in settings of extension (Vendeville and Cobbold, 1988), compression (Davy and Cobbold, 1991; Cobbold et al., 1993; Storti and McClay, 1995; Tondji Biyo, 1995; Barrier et al., 2002; Persson and Sokoutis, 2002), transtension (Dooley and McClay, 1997; Rahe et al., 1998; Schreurs and Colletta, 1998) and transpression (Schreurs and Colletta, 1998; Casas et al., 2001). In all of these settings, sedimentation in the footwall of a fault and erosion of its hanging wall appears to increase the fault dip. For faults with a reverse component of slip, erosion of the hanging wall promotes further slip. Our experiments on strike-slip systems conform to this general pattern, even if the effects of erosion and sedimentation are less pronounced in such a setting, because dip-slip displacements are smaller.

4.2. Dilation in nature and experiment

In all our models, reverse slip on faults resulted from dilation. The free surface allowed the flower structure to pop up, between the bounding reverse faults. The average dilation for the entire flower was about 4%, but it probably reached values of 7% towards the base, where the various fault splays converged. Thus the dilation in each fault splay was probably about 7%. In these models, the reverse faults were not diagnostic of transpression. Can we draw the same conclusions in nature?

For the models to be realistic, it is important that the dilation should be comparable in magnitude to that of brittle rock. In sand, dilation results from changes in the packing of grains, as they slip. We estimated values of up to 7%. In general, the range would appear to be 5–10% (Mandl et al., 1977; Mandl, 1988; Colletta et al., 1991).

In rock, dilation results from micro-faulting, fissuring, or separation at grain boundaries. However, data are scarce. Triaxial experiments have yielded values of 5% for Carrara marble (Fredrich et al., 1989) and 5% for Gebdykes dolomite at zero confining pressure (Yuan and Harrison, 2003). However, 5% may be a minimal value for triaxial tests on rock, because the small size of samples and the rigidity of the compressing pistons probably combine, to inhibit dilation. More generally, triaxial tests may not offer the most favourable conditions for dilation.

In nature, dilation is even more difficult to measure. It requires proper attention to scales and processes. For example, Zaba (1994) estimated the dilation in a single core of veined rock, obtaining a value of 10%. Larger values certainly occur, in situations where a pore fluid pressure maintains open space, so that minerals precipitate from solution.

According to these data, albeit scarce, dilation in the sandbox models may be higher than in nature, but perhaps by no more than a few percent.

4.3. Further comparison of nature and experiment

On comparing our experimental results (Fig. 6) with typical flower structures in nature (Fig. 1), we notice some similarities and some possible differences:

1. In the experiments, where a flower structure formed above a strike-slip fault, the splays had reverse senses of slip. One of the causes was dilation. Thus the reverse faults were not diagnostic of a transpressional environment. We suspect that dilation is also important in natural flower structures, because in some examples, fault offsets increase upward (Fig. 1a). In general, where splays have dominantly reverse senses of slip, we would urge prudence in inferring that the setting was transpressional. However, we would not go as far as to suggest that all positive flower structures result from dilation.
2. In the experiments, under conditions of syn-kinematic sedimentation, earlier splays had gentle dips and did not penetrate the entire layered sequence. This was because the splays became inactive. In contrast, steeper splays reached through the entire sequence, so that the flower structure had the appearance of narrowing upward. The style was a consequence of the transition from R-faults, through P-faults, to Y-faults. However, it was accentuated by erosion of topographic highs and deposition in topographic lows. In nature, flower structures commonly have the same characteristics (Fig. 1a and b).
3. In the experiments, under conditions of syn-kinematic erosion, the central parts of flower structures were subject to rapid uplift and exhumation, and this enhanced the amount

of reverse slip on splays. In nature, eroded strike-slip systems commonly exhibit large components of reverse slip on steep bounding faults (Fig. 1d). Also, deep-seated rocks commonly crop out in the cores of flower structures. In many instances this is due to uplift and exhumation. To what extent the reverse slip is due to dilation remains an open question.

4.4. Limitations of the models

1. Our experiments are relevant to the development of faults in a cover sequence, above a single strike-slip fault in the basement. More complex structures are likely to form, if the basement slips along more than one fault.
2. We did not systematically investigate the effects of mechanical contrasts between layers, as are common in nature. Indeed, few folds developed in our models, whereas they do so readily in models that have alternating layers of sand and viscous material (Richard et al., 1991) and they are common in natural strike-slip systems that develop in well-layered strata (Wilcox et al., 1973; Harding, 1985). In experiments, even a single layer of viscous silicone can cause detachment and so influence the structural development of a flower structure (see Richard et al., 1989).
3. Our models took no account of the effects of fluid overpressure and seepage forces. It is possible to introduce these into sandbox models (Mourgues and Cobbold, 2003) and we would expect them to influence the structural development of strike-slip fault systems.

5. Conclusions

From our five series of experiments on deformation in sand above a strike-slip fault, we draw the following conclusions:

1. In the absence of erosion or sedimentation (Series 1), the structural development was almost identical to that described previously. First to develop were R-faults, striking at about 16° to the basal cut. At later stages of deformation, P-faults and Y-faults took over. In section, faults splayed up from the basal cut, forming flower structures.
2. In all flower structures, faults had reverse components of slip. Reverse slip on fault splays was not a criterion of transpression. Instead it was a result of dilation, which typically averaged about 4% for a whole flower structure, but may have reached values of 7% in fault splays. Areas between R-faults rose, forming topographic highs.
3. In experiments with erosion but no sedimentation (Series 2), faults were less steep, on average. Exhumation of flower structures led to greater amounts of reverse slip on fault splays.
4. In experiments with erosion and sedimentation (Series 3), early faults propagated through their syn-kinematic cover, others became inactive and buried, whilst yet others were exposed by erosion. The average fault dip increased significantly, especially at early and late stages of deformation, and it did not stabilize. The average amount of reverse slip was larger than that of Series 1, but smaller than that of Series 2. This observation may be accounted for by exhumation.
5. In experiments with sedimentation but no erosion (Series 4), some early faults propagated through their syn-kinematic cover, whereas others became inactive and buried. The average fault dip increased steadily and did not stabilize. The average amount of reverse slip on faults was a little larger than that of Series 1, but less than that of Series 3. The increasing thickness of overburden may have suppressed the faults that had gentle dips, whilst favouring the steep faults that had less weight in their hanging walls.

Flower structures in nature have similar features. In areas of syn-kinematic sedimentation, fault splays with gentle dips tend to die out at depth, whereas steeper faults penetrate higher. In areas of erosion, strike-slip systems commonly exhibit large amounts of reverse slip on steep bounding faults and deep-seated rocks crop out in the cores of flower structures as a result of uplift and exhumation. To what extent in nature are components of reverse slip due to dilation? This remains an open question.

Acknowledgements

The experiments were done in the Analogue Modelling Laboratory, Geosciences-Rennes. We are grateful to Jean-Jacques Kermarrec for invaluable help with apparatus. For useful discussions on dilatancy and on strike-slip faults in sand and rock, we thank R.W. Krantz (Conoco-Philips, Houston) and William A. Olsson (Sandia National Laboratories, Albuquerque). Reviewers Joao Keller and John Waldron provided valuable comments and suggestions, which led to an improved manuscript.

References

- Audemard, M.F.A., 1996. Paleoseismicity studies on the Oca–Ancón fault system, northwestern Venezuela. *Tectonophysics* 259, 67–80.
- Barrier, L., Nalpas, T., Gapais, D., Proust, J.-N., Casas, A., Bourquin, S., 2002. Influence of syntectonic sedimentation on thrust geometry. Field examples from the Iberian Chain (Spain) and analogue modelling. *Sedimentary Geology* 146, 91–104.
- Casas, A.M., Gapais, D., Nalpas, T., Besnard, K., Roman-Berdiel, T., 2001. Analogue models of transpressive systems. *Journal of Structural Geology* 23, 733–743.
- Christie-Blick, N., Biddle, K.T., 1985. Deformation and basin formation along strike-slip faults. In: Biddle, K.T., Christie-Blick, N. (Eds.), *Strike-Slip Deformation, Basin Formation, and Sedimentation Society of Economic Paleontologists and Mineralogists Special Publication* 37, pp. 1–34.
- Cloos, H., 1928. Experimente zur inneren Tektonik. *Zentralblatt für Mineralogie, Geologie und Paläontologie* 1928B, 609–621.
- Cobbold, P.R., Davy, P., 1988. Indentation tectonics in nature and experiment. 2. Central Asia. *Bulletin of the Geological Institutions of Uppsala, New Series* 14, 143–162.

- Cobbold, P.R., Davy, P., Gapais, D., Rossello, E.A., Sadybakasov, E., Thomas, J.C., Tondji Biyo, J.J., de Urreiztieta, M., 1993. Sedimentary basins and crustal thickening. *Sedimentary Geology* 86, 77–89.
- Colletta, B., Letouzey, J., Pinedo, R., Ballard, J.F., Balé, P., 1991. Computerized X-ray tomography analysis of sandbox models: examples of thin-skinned thrust systems. *Geology* 19, 1063–1067.
- Crowell, J.C., 1982. The tectonics of Ridge Basin, southern California. In: Crowell, J.C., Link, M.H. (Eds.), *Geologic History of Ridge Basin, Southern California*. Society of Economic Paleontologists and Mineralogists, Pacific Section, pp. 25–42.
- Davy, P., Cobbold, P.R., 1988. Indentation tectonics in nature and experiment. Experiments scaled for gravity. *Bulletin of the Geological Institutions of the University of Uppsala, New Series* 14, 129–141.
- Davy, P., Cobbold, P.R., 1991. Experiments on shortening of a 4-layer model of the continental lithosphere. *Tectonophysics* 188, 1–25.
- Dooley, T., McClay, K., 1997. Analog modeling of pull-apart basins. *American Association of Petroleum Geologists Bulletin* 81, 1804–1826.
- Ellis, S., Schreurs, G., Panien, M., 2004. Comparisons between analogue and numerical models of thrust wedge development. *Journal of Structural Geology* 26, 1659–1675.
- Emmons, R.C., 1969. Strike-slip rupture patterns in sand models. *Tectonophysics* 7, 71–87.
- Fredrich, J.T., Evans, B., Wong, T.F., 1989. Micromechanics of the brittle to plastic transition in Carrara marble. *Journal of Geophysical Research* 94, 4129–4145.
- Harding, T.P., 1985. Seismic characteristics and identification of negative flower structures, positive flower structures, and positive structural inversion. *American Association of Petroleum Geologists Bulletin* 69, 582–600.
- Harding, T.P., 1990. Identification of wrench faults using subsurface structural data: criteria and pitfalls. *American Association of Petroleum Geologists Bulletin* 74, 1590–1609.
- Horsfield, W.T., 1977. An experimental approach to basement-controlled faulting. *Geologie en Mijnbouw* 56, 363–370.
- Hubbert, M.K., 1937. Theory of scale models as applied to the study of geologic structures. *Geological Society of America Bulletin* 48, 1459–1520.
- Mandl, G., 1988. *Mechanics of Tectonic Faulting. Models and Basic Concepts*. Elsevier, 407pp.
- Mandl, G., de Jong, L.N.J., Maltha, A., 1977. Shear zones in granular material. *Rock Mechanics* 9, 95–144.
- Mart, Y., Ryan, W.B.F., Lunina, O.V., 2005. Review of the tectonics of the Levant Rift system: the structural significance of oblique continental breakup. *Tectonophysics* 395, 209–232.
- McClay, K.R., Whitehouse, P.S., Dooley, T., Richards, M., 2004. 3D evolution of fold and thrust belts formed by oblique convergence. *Marine and Petroleum Geology* 21, 857–877.
- Mourgues, R., Cobbold, P.R., 2003. Some tectonic consequences of fluid overpressures and seepage forces as demonstrated by sandbox modelling. *Tectonophysics* 376, 75–97.
- Naylor, M.A., Mandl, G., Sijpesteijn, C.H.K., 1986. Fault geometries in basement-induced wrench faulting under different initial stress states. *Journal of Structural Geology* 8, 737–752.
- Persson, K.S., Sokoutis, D., 2002. Analogue models of orogenic wedges controlled by erosion. *Tectonophysics* 356, 323–336.
- Rahe, B., Ferrill, D.A., Morris, P.A., 1998. Physical analog modeling of pull-apart basin evolution. *Tectonophysics* 285, 21–40.
- Richard, P., 1990. Champs de failles au dessus d'un décrochement de socle: modélisation expérimentale. *Mémoires et Documents du Centre Armoricaïn d'Etude Structurale des Socles* 34, 1–342.
- Richard, P., Cobbold, P.R., 1989. Structures en fleur positives et décrochements crustaux: modélisation analogique et interprétation mécanique. *Comptes Rendus de l'Académie des Sciences de Paris, Série II* 308, 553–560.
- Richard, P., Cobbold, P.R., 1990. Experimental insights into partitioning of fault motions in continental convergent wrench zones. *Annales Tectonicae* 4, 35–44.
- Richard, P., Ballard, J.F., Colletta, B., Cobbold, P.R., 1989. Naissance et évolution de failles au-dessus d'un décrochement de socle: modélisation analogique et tomographie. *Comptes Rendus de l'Académie des Sciences de Paris Série II* 309, 2111–2118.
- Richard, P., Mocquet, B., Cobbold, P.R., 1991. Experiments on simultaneous faulting and folding above a basement wrench fault. *Tectonophysics* 188, 133–141.
- Richard, P.D., Naylor, M.A., Koopman, A., 1995. Experimental models of strike-slip tectonics. *Petroleum Geoscience* 1, 71–80.
- Riedel, W., 1929. *Zur Mechanik geologischer Brucherscheinungen*. *Zentralblatt für Mineralogie, Geologie und Paläontologie* 1929B, 354–368.
- Schöpfer, M.P.J., Steyrer, H.P., 2001. Experimental modeling of strike-slip faults and the self-similar behavior. In: Koyi, H.A., Mancktelow, N.S. (Eds.), *Tectonic Modelling: A Volume in Honor of Hans Ramberg*. Geological Society of America Memoir 193, pp. 21–27.
- Schreurs, G., Colletta, B., 1998. Analogue modelling of faulting in zones of continental transpression and transtension. In: Holdsworth, R.E., Strachan, R.A., Dewey, J.F. (Eds.), *Continental Transpressional and Transtensional Tectonics*. Geological Society of London Special Publication 135, pp. 59–79.
- Skempton, A.W., 1966. Some observations on tectonic shear zones. *First International Congress on Rock Mechanics, Proceedings, Lisbon* 1, 329–335.
- Storti, F., McClay, K., 1995. Influence of syntectonic sedimentation on thrust wedges in analogue models. *Geology* 23, 999–1002.
- Sture, S., Costes, N.C., Batiste, S.N., Lankton, M.R., AlShibli, K.A., Jeremic, B., Swanson, R.A., Frank, M., 1988. Mechanics of granular materials at low effective stresses. *Journal of Aerospace Engineering* 11, 67–72.
- Sylvester, A.G., 1988. Strike-slip faults. *Geological Society of America Bulletin* 100, 1666–1703.
- Tchalenko, J.S., 1970. Similarities between shear zones of different magnitudes. *Geological Society of America Bulletin* 81, 1625–1640.
- Tondji Biyo, J.J., 1995. Chevauchements et basins compressifs. Influence de l'érosion et de la sédimentation. *Modélisation analogique et exemples naturels*. *Mémoires de Géosciences-Rennes* 59, 1–411.
- Umhoefer, P.J., 2000. Where are the missing faults in translated terranes? *Tectonophysics* 326, 23–35.
- Vendeville, B., Cobbold, P.R., 1988. How normal faulting and sedimentation interact to produce listric fault profiles and stratigraphic wedges. *Journal of Structural Geology* 10, 649–659.
- Viola, G., Odonne, F., Mancktelow, N.S., 2004. Analogue modelling of reverse fault reactivation in strike-slip and transpressive regimes: application to the Giudicarie fault system, Italian Eastern Alps. *Journal of Structural Geology* 26, 401–418.
- Wilcox, R.E., Harding, T.P., Seely, D.R., 1973. Basic wrench tectonics. *American Association of Petroleum Geologists Bulletin* 57, 74–96.
- Yuan, S.-C., Harrison, J.P., 2003. An empirical dilatancy index for the dilatant deformation of rock. *International Journal of Rock Mechanics & Mining Sciences* 41, 679–686.
- Zaba, J., 1994. Mesoscopic flower structures in the lower Paleozoic deposits of the NE margin of the Upper Silesian coal basin from transpressional shearing in the Cracow Myszkow (Hamburg-Cracow) dislocation zone. *Przegląd Geologiczny* 42, 643–648 (in Polish, with English abstract).